# Numerical Study of Outlet Pressure on the Condensing Flow from Steam Turbine Blade with Blade Spacing Variation

Nauvilah Virganata, Lohdy Diana* and Arrad Ghani Safitra†

*Power Plant Engineering, Politeknik Elektronika Negeri Surabaya, Surabaya, Indonesia*

Keywords:     Simulation, Steam Turbine, Condensing, CFD.

Abstract:     Condensation occurring in low-pressure stages of steam turbines contributes to many losses in efficiency. Condensation is changing the vapor phase to the liquid phase due to pressure and temperature below saturation. This research aims to simulate the condensation at the last stage of the steam turbine to understand the phenomenon with blade spacing variation. Numerical simulation was conducted by using CFD Fluent. The expected result is that the greater the distance between the blades, the smaller the chance of condensation. It is evident at the P = 91.74 spacing variation has a minimum pressure 22kPa and the lowest droplet growth rate of 1212.663 microns/s.

## 1 INTRODUCTION

The steam turbine's function is to convert thermal energy. The water vapor that has been heated in the boiler into mechanical energy in the form of a rotation which can then rotate the generator shaft and produce electrical energy in the generator (Manushin, 2011). PLTU usually has three levels of turbines based on their pressure, namely high-pressure steam turbines, medium steam turbines, and the last stage, low-pressure steam turbines (Syahputra et al., 2019).

One of the problems in the low-pressure steam turbine is the formation of dew in the form of tiny water droplets called a condensation vapor flow (Buckley, 2003). The condensation process is caused by a decrease in pressure and temperature, which causes tiny water droplets (nucleation) (Jensen et al., 2014). There are two kinds of nucleated, namely homogenous, where the water droplets have almost the same density and heterogeneous (Wood et al., 2002). The condensation process occurs at the last stage due to the external pressure, which the condenser should overcome (Cao et al., 2020). As a result of the condensed steam flow, it can cause corrosion and holes in the blade. Besides that, there are several other losses such as erosion due to water drops formed and moving to the blade material and the turbine casing, thermodynamic losses due to the cooling effect due to the presence of fluids, and aerodynamics due to collisions between the liquid phase and blade material (Jonas & Machemer, 2008).

Ahmed M. Nagib Elmekawy, Mohey Eldeen H. H. Al. (2019), "Computational modeling of non-equilibrium condensing steam flows in a low-pressure steam turbine." This journal discusses the simulation of condensation phenomena on a steam turbine blade in the last stage using CFD software (Diana et al., 2019). According to the geometry journal will affect the value of the blade exit speed. The higher the flow rate causes a significant decrease in pressure and temperature, which causes an increase in the mass fraction of the liquid so that there will be increased condensation in the blade exit area (Nagib Elmekawy & Ali, 2020).

Based on the importance of the effect of the condensation flow on the performance of the steam turbine, in this research, the researcher will simulate the condensation flow on the stator blade with four cascade blades, which produces three blade to blade channels with variations in the distance between the blades, namely 91.74 mm and 70.5 mm at the final stage of a low-pressure steam turbine.

---

* https://www.scopus.com/authid/detail.uri?authorId=57
  206902929

† https://www.scopus.com/authid/detail.uri?authorId=56
  013168800

This research will predict the distribution of static pressure that most affects the phase to determine the droplet formed and the efficiency.

# 2 NUMERICAL METHOD

The steam turbine blade design will be made using a commercial CFD with 2D drawings to see the flow in the final stage of the steam turbine stator blade.

## 2.1 Geometry

Geometry In this research, 2D is made with the domain in a fluid with the geometric data in the table below.

Table 1: Blade Geometry.

| No | Pressure Side | | Suction Side | |
|----|-------|--------|-------|--------|
| | X (mm) | Y (mm) | X (mm) | Y (mm) |
| 1 | 0 | 143.45 | 0 | 143.45 |
| 2 | 14.1 | 132.95 | 14.47 | 156.15 |
| 3 | 28.3 | 132.3 | 30.55 | 160.71 |
| 4 | 42.38 | 130.19 | 47.46 | 163.46 |
| 5 | 56.16 | 126.65 | 64.59 | 162.75 |
| 6 | 69.52 | 121.72 | 81.21 | 158.12 |
| 7 | 82.28 | 115.45 | 96.36 | 150.05 |
| 8 | 94.35 | 107.91 | 109.68 | 139.29 |
| 9 | 105.63 | 99.14 | 120.74 | 126.24 |
| 10 | 116.23 | 89.5 | 129.5 | 111.89 |
| 11 | 126.23 | 79.17 | 137.49 | 97.34 |
| 12 | 135.57 | 68.23 | 144.97 | 82.5 |
| 13 | 140.02 | 62.51 | 148.52 | 74.95 |
| 14 | 144.22 | 56.7 | 151.91 | 67.4 |
| 15 | 148.25 | 50.76 | 155.19 | 59.74 |
| 16 | 152.05 | 44.76 | 158.29 | 52.1 |
| 17 | 155.66 | 38.65 | 161.28 | 44.37 |
| 18 | 159.08 | 32.43 | 164.1 | 36.66 |
| 19 | 162.38 | 26 | 166.8 | 28.85 |
| 20 | 162.45 | 19.41 | 169.36 | 20.99 |

In this research, blade spacing variations were carried out by increasing and decreasing space from the original size. The blade spacing variations were 91.74 mm and 70.5 mm.
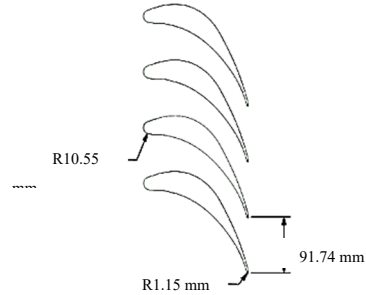


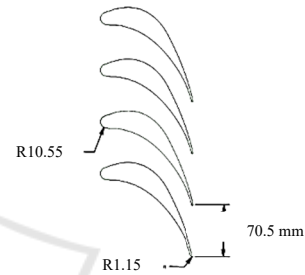Figure 1: Blade Geometry with Blade Spacing 91.74 mm.



Figure 2: Blade Geometry with Blade Spacing 70.5 mm.

## 2.2 Meshing

In this study, meshing was carried out using ICEM CFD. We want to analyze the wall blade, and the mesh is reduced to get better results. The local mesh used in this study is sizing. The meshing chosen for this study resulted in 45481 elements and 46280 nodes with a minimum skewness of 0.3.
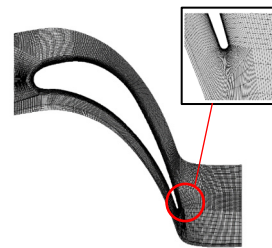


Figure 3: Meshing.

Table 2: Boundary Condition.

| No. | Description | Value | Unit |
|-----|-------------|-------|------|
| 1 | Pressure Inlet | 89 | kPa |
| 2 | Pressure Outlet | 39 | kPa |
| 3 | Temperature Inlet | 100 | ºC |

## 2.3 Processing

This stage relates to determining the boundary conditions in a CFD simulation. The wet steam approach has been used for multiphase modeling, and the k- ω SSt is used in the viscous model, while the density-based and steady-state are used for the solution setup in the solver model.

## 2.4 Equation

The condensation occurs due to a decrease in pressure below saturation until the vapor changes from gas to liquid form.

$$\beta = \frac{m_l}{m_l + m_v} = \frac{\alpha_l \rho_l}{\alpha_l \rho_l + (1 - \alpha_l)\rho_v} \tag{1}$$

$\beta = liquid\ mass\ fraction$

$m_l = massa\ liquid$

$m_v = massa\ vapor$

$\alpha_l = volume\ fraction\ liquid$

$\rho_v = densitas\ vapor$

$\rho_l = densitas\ liquid$

The condensation process begins with a nucleation process with tiny water droplets due to decreased pressure and temperature. The water droplets can enlarge as in classical nucleation theory, or the water droplets can return to steam.

$$J = \frac{q_c}{1+\theta}\left(\frac{\rho_v^2}{\rho_l}\right)\sqrt{\frac{2\sigma}{\pi M^3}}\,e^{-\left(\frac{4\pi r_*^2 \sigma}{3k_B T}\right)} \tag{2}$$

J   = Nucleation rate $\left(\frac{l}{m^3 s}\right)$

M  = Water mass molecul (kg)

$k_B$ = Boltzman constanta

$T_v$ = Steam temperature (K)

$\rho_v$ = Steam density $\left(\frac{kg}{m^3}\right)$

$\rho_l$ = Liquid density $\left(\frac{kg}{m^3}\right)$

$q_c$ = Condensation Coefficient

$\sigma$  = Surface tension $\left(\frac{N}{m}\right)$

$\theta$  = Correction factor non-isotermal

Critical radius of droplet:

$$r_* = \frac{2\sigma}{\rho_l RT lnS} \tag{3}$$

r   = Droplet radius (m)

$\sigma$   = Liquid surface tension $\left(\frac{N}{m}\right)$

R    = Gas coefficient $\left(\frac{J}{kgK}\right)$

$\rho_l$   = Liquid density $\left(\frac{kg}{m^3}\right)$

T    = Temperature (K)

Condensation also affects turbine efficiency. The amount of condensation can cause a decrease in efficiency and erosion.

$$\eta_s = \frac{h_{in} - h_{out}}{h_{in} - h_{out,s}} \tag{4}$$

$h_{in}$ = entalpi pada sisi inlet

$h_{out}$ = entalpi pada sisi outlet

$h_{out,s}$ = entalpi issentropis pada sisi stator

$\eta_s$ = efisiensi isentropis

## 3 RESULT AND DISCUSSION

## 3.1 Grid Independent

The independent grid in this research has been done by meshing periodically to get the meshing with the slightest possible error.

Table 3: Mesh Variation.

| Number of Elements | Type | Average of Static Pressure | Error Mesh |
|---|---|---|---|
| 33616 | A | 65176.80 | - |
| 41161 | B | 64943.81 | 0.1291 |
| 45481 | C | 64001.76 | 1.4595 |
| 58998 | D | 64023.91 | 0.0346 |
| 60248 | E | 64026.26 | 0.0037 |

There are five mesh variations mesh A with 33616 cells, mesh B with 41161 cells, mesh C with 45481 cells, mesh D with 58998 cells, and mesh E with 60248 cells. The results show that the mesh variation C has a static pressure starting to be constant. Compared to the mesh variations, D and E variation C has the least number of cells, so that the simulation will be efficient.
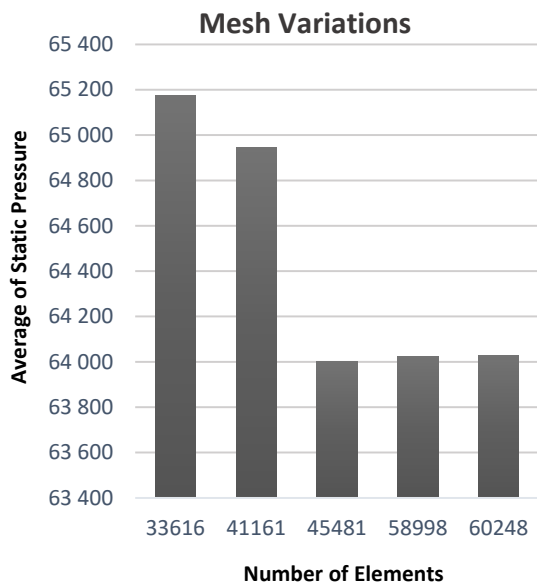
Figure 4: Result of Mesh Independent.

## 3.2 Validation

Validation using a mesh with variation C has several elements measuring 45481 with an average statistical pressure of 64001.76423 Pa. This value is then compared with the statistical pressure value on the quoted paper to calculate the error value. The numerical study is valid if the error is below 3%, and in Table 4, it is shown that the average error obtained is 2.9%, so that the simulation in this research is valid.

Table 4: Validation of Static Pressure.

| Pressure Side | | | |
|---|---|---|---|
| X | Experiment (Pa) | Simulation (Pa) | Error (%) |
| 0.10563 | 79131.3 | 79461 | 0.416649 |
| 0.11623 | 76537.4 | 76708.7 | 0.354931 |
| 0.12624 | 72767.3 | 73694.4 | 1.274061 |
| 0.13557 | 70497.3 | 70893.8 | 0.562433 |
| 0.14001 | 68161.1 | 69764.9 | 2.352955 |
| 0.14422 | 67068.2 | 68689.7 | 2.417688 |
| 0.14825 | 66396.5 | 67727.5 | 2.004624 |
| 0.15205 | 66573.9 | 67497.8 | 1.387781 |
| 0.15566 | 66396.5 | 67015..4 | 0.932127 |
| 0.15908 | 65508.5 | 66472.1 | 1.470954 |
| 0.16236 | 64718.5 | 65631.6 | 1.410879 |
| 0.16545 | 63417.8 | 64284.7 | 1.366966 |

| Suction Side | | | |
|---|---|---|---|
| X | Experiment (Pa) | Simulation (Pa) | Error (%) |
| 0.08121 | 71100.2 | 71579.2 | 0.673697 |
| 0.09636 | 66296.7 | 67192.3 | 1.350897 |
| 0.10968 | 60392 | 61479.5 | 1.800735 |
| 0.12074 | 57260.1 | 59292.1 | 3.548719 |
| 0.1295 | 60608.2 | 61494.4 | 1.462178 |
| 0.13749 | 58726 | 59813.4 | 1.85165 |
| 0.14497 | 53188.3 | 53188.3 | 0 |
| 0.14852 | 47504.6 | 47504.6 | 0 |
| 0.15191 | 42063.2 | 46522.3 | 10.60095 |
| 0.15519 | 48070 | 45783.6 | 4.756397 |
| 0.15829 | 45328.2 | 40732.1 | 10.1396 |
| 0.16128 | 42593 | 38080.2 | 10.59517 |
| 0.1641 | 38804.2 | 35829.5 | 7.665923 |
| 0.1668 | 36061.8 | 34476.5 | 4.396065 |
| 0.16936 | 34044.1 | 32705.1 | 3.933134 |
| Average of error | | 2.915821 | |

## 3.3 The Effect of Blade Spacing Variations

Condensation occurs when the vapor goes through the expansion process so that the static pressure drops below the saturation pressure, which causes a phase change from the vapor phase to the liquid phase (Nagib Elmekawy & Ali, 2020).

The value of static pressure on the variation of the blade spacing P = 91.74 mm, and P = 70.5 mm is shown in Fig. 4. Static pressure contours show that changes in blade distance affect the distribution of static pressure, especially in the trailing edge area. The static pressure contour shows that the pressure at the inlet blade is greater than the outlet pressure. The lowest pressure drop value was obtained in the most significant variation of blade distance P = 91.74 mm, while the slightest variation of blade distance P = 70.5 mm had the highest pressure drop. The smaller the blade distance, the smaller the cross-sectional area of the flow and increases the rate of steam expansion so that there is a greater chance of condensation.
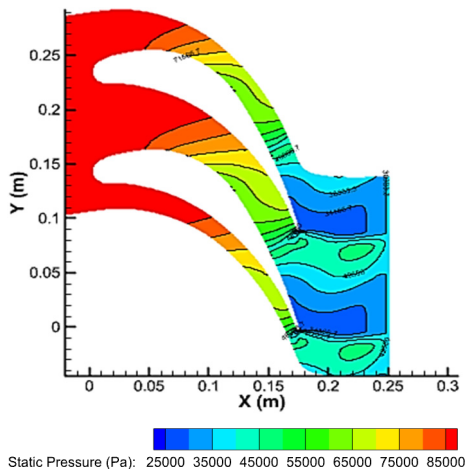
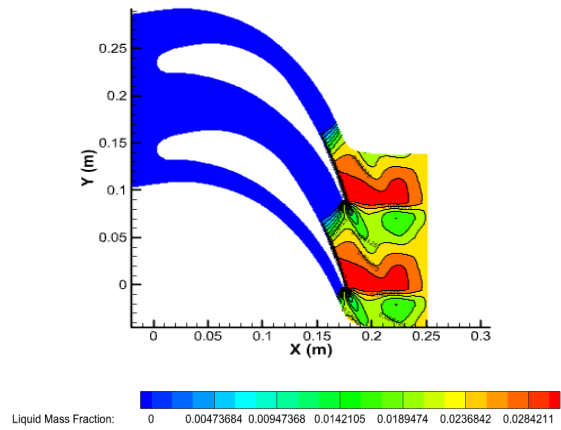Figure 5: Contour of static pressure (Pa) for blade spacing P = 91.74 mm.



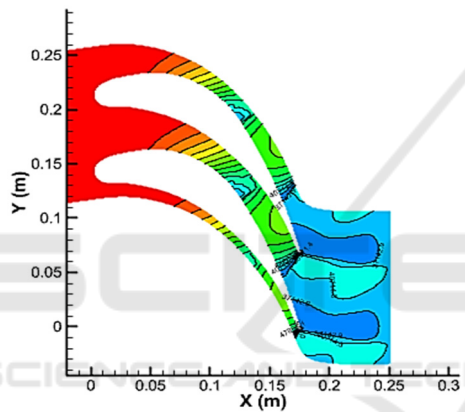Figure 7: Contour of liquid mass fraction for blade spacing P = 91.74 mm.



Figure 6: Contour of static pressure (Pa) for blade spacing P = 70.5 mm.



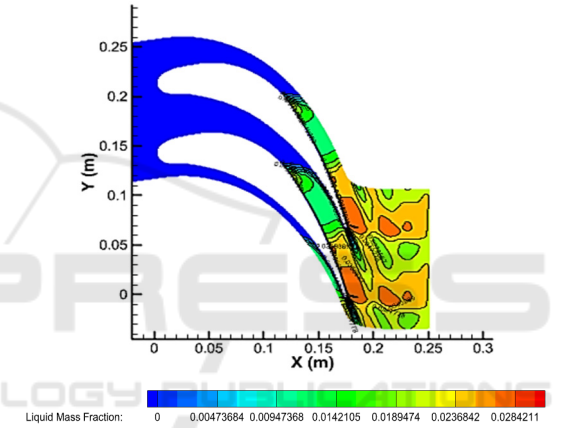Figure 8: Contour of liquid mass fraction for blade spacing P = 70.5 mm.

The liquid mass fraction contour describes the state of the vapor in the gap between the blades. The liquid fraction in Fig. 5 is found around the trailing edge. It is because the rate of steam expansion in the area has the highest value. The contours of the liquid mass fraction for various blade spacing variations are P = 91.74 mm, and P = 70.5 mm. It can be seen that the smaller the distance between the blades, the more liquid fraction is formed. In the variation of the blade distance, P = 70.5 mm has the most liquid mass fraction, which is indicated by more areas that have a fraction value of more than 0, which reflects that much water is formed compared to other variations. In addition, as the blade spacing widens, the zone with a value greater than 0 becomes narrower.

The droplet growth rate is the number of droplets produced every second. From the droplet growth rate contours in Fig. 6, it can be seen that variations in blade distance can affect the speed of droplet formation in the blade gap. In the variation, P = 91.74 mm has a maximum droplet growth rate of 1212.663 microns/s; at variation, P = 70.5 mm has a maximum droplet growth rate of 1280.906 microns/s. Then the variation of the distance P = 91.74 mm, and P = 70.5 mm, it is known that the smaller the distance between the blades, the higher the droplet formation speed. It can be seen in the droplet growth rate contour at variation P = 70.5 mm, which has many red zones, while at variation P = 91.74 mm has the lowest droplet growth rate, which is indicated by the minor red zones. When compared to each variation, the highest droplet growth was in the P = 70.5 mm variation with a maximum velocity value of 1280,906 microns/s.
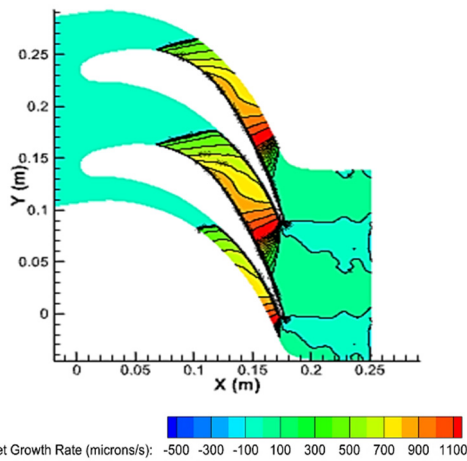
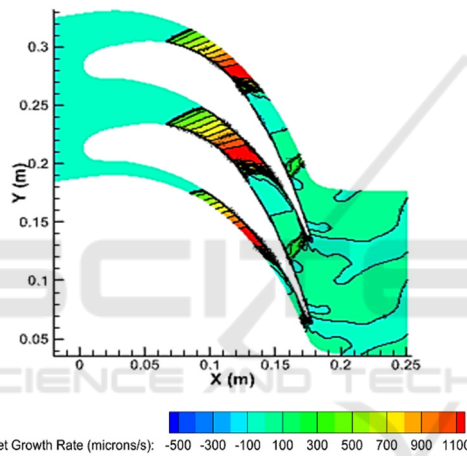Figure 9: Contour of droplet growth rate (microrns/s) for blade spacing P = 91.74 mm.



Figure 10: Contour of droplet growth rate (microrns/s) for blade spacing P = 70.5 mm.

Variations in the distance between blades affect the droplet radius. In Fig. 7, The variation of P = 91.74 mm has the lowest droplet radius, while the variation of distance P = 70.5 mm has the largest droplet radius. It shows that the smaller the distance between the blades, the greater the droplet growth rate according to the droplet growth rate contour. When compared with distance variations, it can be seen that the smaller the distance between the blade radius formed, the larger the radius. The 70.5 mm variation has the most considerable minimum radius value of 0.01 microns. It is because the pressure on the mainstream blade with a smaller distance will also be smaller.
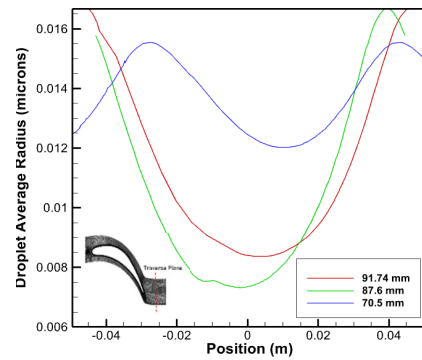


Figure 11: Graph of droplet average radius (microrns) for blade spacing variations.

Table 5 is the result of calculating the isentropic efficiency of the blade. The calculation of isentropic efficiency is carried out to determine the effect of the distance between blades on efficiency. It is known that the distance between blades can affect isentropic efficiency. The smaller the distance between the blades, the smaller the isentropic efficiency of the blade. At a distance of P = 91.74mm, the highest efficiency is 88.06 %, and at a distance of P = 70.5 mm, the lowest efficiency is 85.37%. It is caused by the outlet pressure getting smaller and the smaller variations in the distance between the blades.

Table 5: Isentropic Efficiency.

| Blade Spacing Variation | Outlet Pressure (kPa) | Isentropic Efficiency (%) |
|---|---|---|
| P = 91.74 mm | 39.25 | 88.06 |
| P = 70.5 mm | 39.07 | 85.37 |

## 4 CONCLUSIONS

The blade stator is simulated by numerical simulation with Computational Fluid Dynamic (CFD) with variations in blade distance resulting in the following main conclusions. Variations in the distance between blades affect the distribution of static pressure on the steam flow. The blade with a distance of P = 70.5 mm has the highest expansion rate because it has the lowest minimum pressure of 13703.65 Pa and variations in the distance between blades affect the formation of condensation, which can be seen from the contours of the liquid mass fraction. The blade with the smallest distance P = 70.5 mm has a liquid mass fraction zone and has a widest value of more than 0, which means more condensate is formed also

can be seen from the droplet growth contour. The blade with the smallest distance P = 70.5 mm has the highest droplet formation speed of 1280.906 microns/s. The average droplet radius graph shows variations with the smallest distance P = 70.5 mm having the largest droplet radius with a minimum of 0.01 microns and the isentropic efficiency table shows the variation with the lowest efficiency at variation P = 70.5 mm by 85.37%he blade spacing variation affects the distribution of static pressure on the steam flow, where the blade with the smallest distance P = 70.5 mm has the highest expansion rate compared to other variations.

## ACKNOWLEDGEMENTS

## REFERENCES

Buckley, J. R. (2003). *A Study of Heterogeneous Nucleation and Electrostatic Charge in Steam Flows. November.*

Cao, L., Wang, J., Luo, H., Si, H., & Yang, R. (2020). Distribution of condensation droplets in the last stage of steam turbine under small flow rate condition. *Applied Thermal Engineering*, *181*(September), 116021. https://doi.org/10.1016/j.applthermaleng.20 20.116021

Diana, L., Safitra, A. G., & Muhammad, G. (2019). Numerical Investigation of Airflow in a Trapezoidal Solar Air Heater Channel. *IES 2019 - International Electronics Symposium: The Role of Techno-Intelligence in Creating an Open Energy System Towards Energy Democracy, Proceedings*, 248–253. https://doi.org/10.1109/ELECSYM.2019.8901524

Jensen, K. R., Fojan, P., Jensen, R. L., & Gurevich, L. (2014). Water condensation: A multiscale phenomenon. *Journal of Nanoscience and Nanotechnology*, *14*(2), 1859–1871. https://doi.org/10.1166/jnn.2014.9108

Jonas, O., & Machemer, L. (2008). Steam Turbine Corrosion and Deposits Problems and Solutions. *Thirty-Seventh Turbomachinery Symposium*, 211–228.

Manushin, E. A. (2011). Steam Turbine. *A-to-Z Guide to Thermodynamics, Heat and Mass Transfer, and Fluids Engineering*.
https://doi.org/10.1615/atoz.s.steam_turbine

Nagib Elmekawy, A. M., & Ali, M. E. H. H. (2020). Computational modeling of non-equilibrium condensing steam flows in low-pressure steam turbines. *Results in Engineering*, *5*, 100065. https://doi.org/10.10 16/j.rineng.2019.100065

Syahputra, R., Wahyu Nugroho, A., Purwanto, K., & Mujaahid, F. (2019). Dynamic performance of synchronous generator in steam power plant. *International Journal of Advanced Computer Science and Applications*, *10*(12), 389–396. https://doi.org/ 10.14569/ijacsa.2019.0101251

Wood, S. E., Baker, M. B., & Swanson, B. D. (2002). Instrument for studies of homogeneous and heterogeneous ice nucleation in free-falling supercooled water droplets. *Review of Scientific Instruments*, *73*(11), 3988. https://doi.org/10.1063/ 1.1511796